

Regular Article

Tuning electronic properties of boron nitride nanoplate via doping carbon for enhanced adsorptive performance



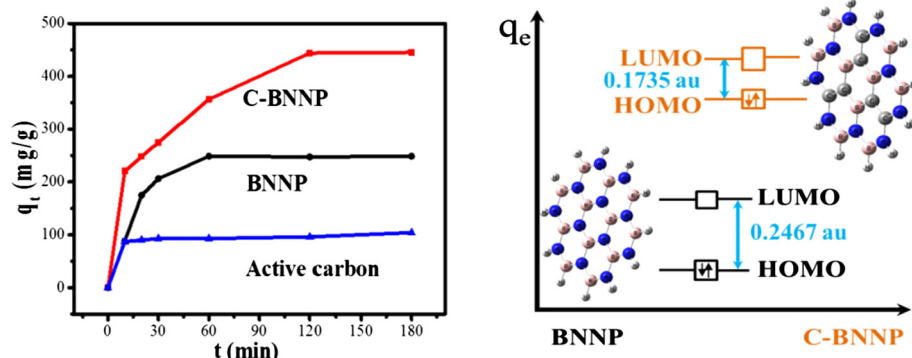
Jingyu Pang^{a,b}, Yanhong Chao^{c,*}, Honghong Chang^b, Hongping Li^b, Jun Xiong^b, Minqiang He^b, Qi Zhang^b, Huaming Li^b, Wenshuai Zhu^{b,*}

^aSchool of Food and Biological Engineering, Jiangsu University, Zhenjiang 212013, PR China

^bSchool of Chemistry and Chemical Engineering, Jiangsu University, Zhenjiang 212013, PR China

^cSchool of Pharmacy, Jiangsu University, Zhenjiang 212013, PR China

GRAPHICAL ABSTRACT



ARTICLE INFO

Article history:

Received 20 April 2017

Revised 14 July 2017

Accepted 3 August 2017

Available online 4 August 2017

Keywords:

Boron nitride

Adsorption

Dyes

Density functional theory

ABSTRACT

In this paper, the carbon-doped boron nitride nanoplate (C-BNNP) was prepared by pyrolyzing the precursor under N_2 and served as an excellent adsorbent for removal of Rhodamine B (RhB). The structure and composition of C-BNNP were characterized and its adsorption behavior for RhB was investigated. Compared with boron nitride nanoplate (BNNP) which was synthesized under NH_3 , C-BNNP displayed an enhancement of the adsorption capacity for RhB (833 mg/g). The adsorption activity was comprehensively studied by kinetics, isotherm and thermodynamics. The adsorption kinetics followed pseudo-second-order model. The equilibrium adsorption data agreed well with the Langmuir isotherm. And the thermodynamics indicated that the adsorption process was a spontaneous, exothermic and physisorption process. In addition, the density functional theory was proposed that doping carbon in the BNNP decreased the chemical hardness of the adsorbent and enhanced the adsorption capacity of C-BNNP for RhB.

© 2017 Published by Elsevier Inc.

1. Introduction

Organic dyes applied widely in the textile, leather, paper industries and food technology are primary pollutants of water environ-

ment [1–3]. Removal of organic dyes is essential because of their potential carcinogenic, toxic, and nonbiodegradable nature. Various methods [4–6] have been developed to remove dyes from contaminated water, among which adsorption proves to be an efficient way due to its simplicity of design, convenient operation and wide suitability for diverse dyes [7–11]. Common adsorbents, including

* Corresponding authors.

E-mail addresses: chaoyh@ujs.edu.cn (Y. Chao), zhuws@ujs.edu.cn (W. Zhu).

activated carbon [12], zeolites [13], and clay [14], suffer from poor specific surface area and low adsorption capacity. Great efforts are made to develop some advanced materials. Indeed, the desired materials should not only exhibit excellent capacity and kinetics, but also be easy to separate from water.

Low-density hexagonal boron nitride (h-BN), so-called 'white graphite', possesses unique properties, including a wide-band gap, low density, electrical insulation, outstanding thermal conductivity [15–17]. In addition, high surface area, high chemical inertness and environmentally friendly characteristics of h-BN provide excellent properties for adsorption [18–20]. Therefore, h-BN is considered as an ideal candidate for adsorption material. Recently, Lei et al. [21,22] synthesized various BN nanosheets and studied the versatile adsorption capacity for oils, proteins, dyes. Tang et al. [23–25] reported diverse BN morphology, such as activated BN, BN fibers and BN foam-like porous monoliths as effective adsorbents to remove organic pollutants. Yu et al. [26] fabricated BN spheres by a catalyzing thermal evaporation method, which showed universal adsorption, such as oil, dyes, and heavy metal ions. However, these works almost focused on the control of morphological features of BN but the adsorption capacity and the adsorption mechanism was not deeply discussed.

In order to further improve the adsorption capacity of BN, the strategy we take is tuning the electronic properties of the adsorbent, namely chemical hardness. Chemical hardness stands for the resistance of the chemical potential to change in the number of electrons. In our previous work [27], the density function theory was investigated and found that adsorption behavior was interrelated to the chemical hardness of the adsorbent, which was also expressed by the HOMO-LUMO gap. Meanwhile, atom doping was an efficient approach to tune the electronic properties of BN [28,29]. In this work, in-situ doping was employed in the synthesis of carbon-doped boron nitride nanoplate (C-BNNP), which was obtained by the pyrolysis of precursors (Dicyanamide and boric acid) under N_2 atmosphere. And the adsorptive performances as well as mechanisms were investigated via batches of adsorption experiments to remove Rhodamine B (RhB) from aqueous systems.

2. Experimental

2.1. Preparation of the adsorbents

Dicyanamide (Dcy) and boric acid (BA) with a molar ratio of 1:3 were dissolved in a mixed solution contains 20 mL water and 20 mL methanol [30], and recrystallized at 55 °C. Then, the received Dcy-BA precursors were pyrolyzed under N_2 at 1000 °C for 5 h with a heating rate of 10 °C/min, the final light yellow powders were marked as carbon-doped boron nitride nanoplate (C-BNNP). Furthermore, nitride nanoplate nanoplate (BNNP) without carbon-doped was synthesized by pyrolyzing the Dcy-BA precursors under NH_3 at 1000 °C for 5 h with a heating rate of 10 °C/min with the appearance of white powders.

2.2. Characterization

The structures of the obtained adsorbents were characterized by Fourier transform infrared spectroscopy (FTIR, Nexus 470, Thermo Electron Corporation), Raman spectroscopy (Raman, Renishaw RM-1000), X-ray diffraction (XRD-6100Lab), UV-vis diffuse reflectance spectroscopy (Shimadzu UV-2450 spectrophotometer), X-ray photoemission spectroscopy (XPS, Kratos Amicus), scanning electron microscopy (SEM, JEOL JSM-7001F) and transmission electron microscopy (TEM, JEOL JEM-2100). The specific surface area

(SSA) of the adsorbents was determined by nitrogen adsorption at 77 K (TriStar II 3020 analyzer).

2.3. Adsorption experiments

Batches of static adsorption experiments were carried out to investigate the adsorption behaviors of RhB onto C-BNNP and BNNP. Typically, 5 mg adsorbent was placed into 25 mL aqueous solutions containing the dye. The concentration of remaining RhB (C_t) at time t was determined by UV-vis spectroscopy. The adsorption capacity q_t and removal efficient (E_t) was calculated as the following equation:

$$q_t = V(C_0 - C_t)/m \quad (1)$$

$$E_t = 100(1 - C_t/C_0) \quad (2)$$

where C_0 (mg/L) was the initial concentration of RhB. V (L) was the volume of the solution, and m (g) was the mass of the adsorbent.

To investigate the adsorption isotherms, 2 mg of adsorbent was added into 10 mL RhB solutions of different initial concentrations (100–300 mg/L) at 298 K until adsorption equilibrium. The concentration of remained RhB (C_e , the C_t at equilibrium) was determined to calculate q_e (the q_t at equilibrium). And adsorption isotherms at different temperatures (298 K, 308 K and 318 K) were also measured to study the adsorption thermodynamics.

2.4. Regeneration performance

The adsorption-desorption cycle experiments were performed by using ethanol as an eluent. C-BNNP saturated with RhB were collected by centrifugation and washed several times with ethanol. After that, the samples were added into ethanol solution for desorption. When reached desorption equilibrium, the adsorbents were collected and reused for adsorption. The whole processes were repeated for 5 times.

3. Results and discussion

3.1. Adsorbent characterization

The structures of C-BNNP and BNNP are investigated by XRD, FTIR and Raman. Fig. 1a shows the XRD pattern of the samples, where the peaks at 26.6, 42.0 can be ascribed to the diffraction of (0 0 2), (1 0 0) planes of hexagonal BN (JCPDS card No. 34-0421), respectively [31]. And the broad peak of (0 0 2) also indicates the poor crystallization of the BN with an interplanar distance of around 0.328 nm obtained by Bragg Equation. Fig. 1b is the FTIR spectrum of the obtained samples. In the spectrum, two strong characteristic bands around 814 cm^{-1} and 1396 cm^{-1} are observed, which ascribed to the out-of-plane bending vibration of sp^2 -bonded B-N-B and the in-plane stretching vibration of sp^2 -bonded B-N, respectively [32]. In addition, several weak bands are also observed. The bands at 2875 cm^{-1} and 2933 cm^{-1} are attributed to the B-NH₂ groups and the one at 3450 cm^{-1} is attributed to the B-OH group [33]. As shown in Fig. 1c, the Raman spectrum shows the obvious BN E_{2g} peak at about 1374 cm^{-1} . According to the XRD, FTIR and Raman spectra, the unchanged characteristic peaks are observed in both C-BNNP and BNNP, indicating that the original BN framework is remained.

The obtained C-BNNP morphology is analyzed by SEM and TEM (Supplementary Material Fig. S1). The SEM image of C-BNNP exhibits irregular shape and twisted polygon appeared with the sizes varying from 1 μm to 6 μm . The detailed TEM image shows

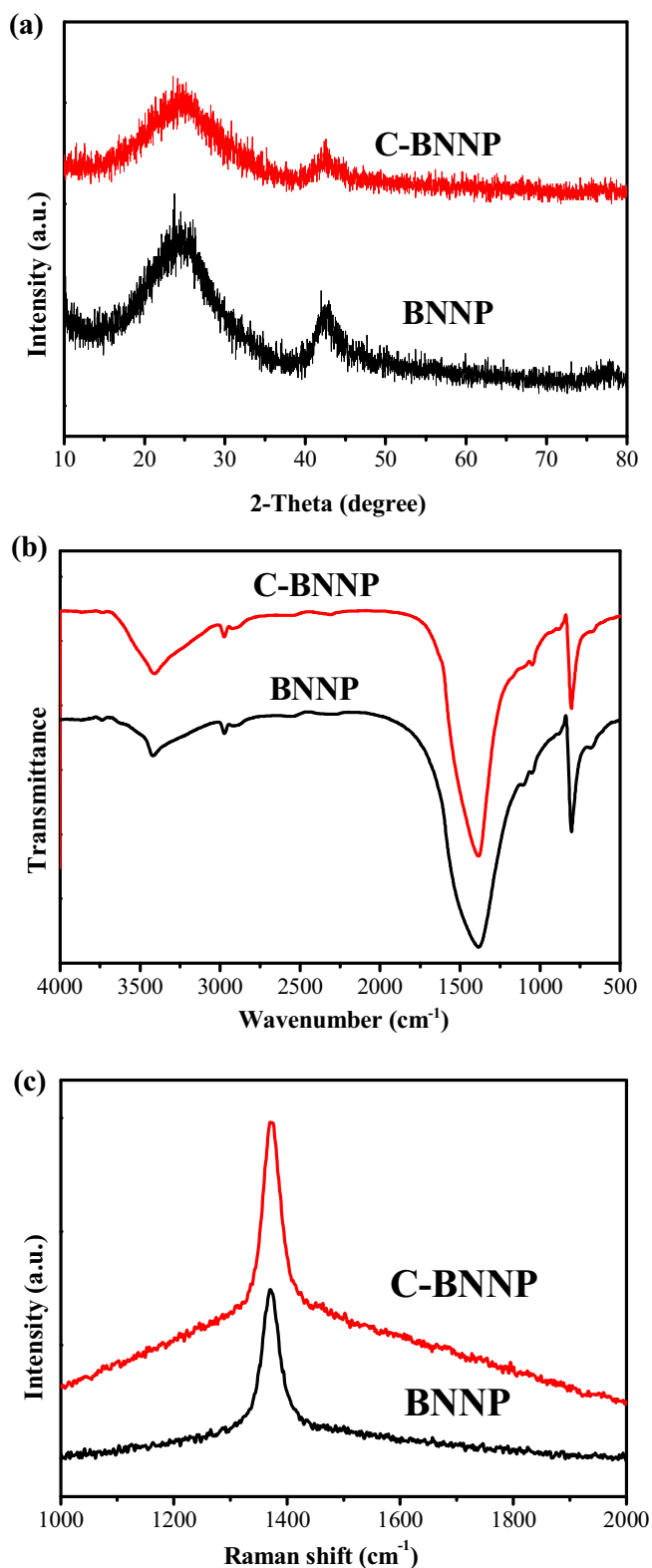


Fig. 1. XRD pattern (a), FTIR spectrum (b), Raman spectrum (c) of the C-BNNP and BNNP.

obvious presence of micropores in the obtained C-BNNP. The N_2 adsorption-desorption isotherms of the C-BNNP and BNNP in [Supplementary Material Fig. S2](#) can closely be classified as type I and H4 hysteresis loops. The similar curves indicate that the structure of pore was maintained when carbon atom doped. And the main

porosities of the investigated samples belong to micropores ($0.26\text{--}0.37\text{ cm}^3/\text{g}$, [Supplementary Material Table S1](#)), which are in accordance with the TEM observations.

The composition of C-BNNP is further obtained via UV-vis DRS analysis, EDS mapping of SEM and XPS. The UV-vis DRS of the C-BNNP and BNNP is shown in [Fig. 2a](#). In the spectrum, the same adsorption peak of C-BNNP and BNNP are observed at 241 nm corresponds to the band gap transition adsorption of h-BN [34]. Compared to BNNP, it's noteworthy that the UV-vis DRS adsorption edges of the hybrid materials of C-BNNP shift to a higher wavelength. And the tail peak is attributed to the carbon doping [35,36]. In [Fig. 2b](#), many randomly polygonal are pieced together. The corresponding DES mapping images of C-BNNP are displayed in [Fig. 2c–e](#). The three color mapping images, red B-K, green C-K and yellow N-K, prove the generally uniform distribution of B, C, N elements.

X-ray photoelectron spectroscopic studies are further performed to evaluate the C in the BNNP. And the results are summarized in [Fig. 3](#). The atomic percentage of B, C, and N in the as-prepared C-BNNP product is calculated from the XPS survey spectrum ([Fig. 3a](#)) to be around 35%, 19%, and 32%, respectively. The oxygen signal around 540 eV is possibly due to the B-OH, which is further proved by FTIR at the peak of 3450 cm^{-1} . The high-resolution and deconvoluted B 1s XPS spectrum given in [Fig. 3b](#) shows mainly two subpeaks at 190.5 and 192.8 eV, arising from the B-N and B-O bond, respectively. The high-resolution N 1s XPS peak in [Fig. 3c](#) can be fitted with three subpeaks at 397.8, 398.7, and 399.3 eV, attributing to the N-B bond, graphitic N-C bond, and pyridinic N-C bond, respectively [37]. The amount of pyridinic N is relatively smaller than the graphitic N. The predominant asymmetric C 1s peak shown in [Fig. 3d](#) indicates the existence of C-N or C-B bonds in the graphitic network. The four deconvoluted peaks in the C 1s spectrum at 283.8, 284.8, 286.1, and 288.4 eV can be assigned to C-B, C-C, C-N, and C-O bonds, respectively [37,38]. Based on the above analysis, the formation mechanism we proposed is that carbon-doped boron nitride nanoplate is formed by the attachment of boron acid molecules to the edge of the dicyanamide and rearrangement, considering dicyanamide as initial seed, is favorable through the edge. Through the subsequent self-assembly and structure optimization, then the carbon-doped boron nitride is formed, which is similar to the formation of previous reports [17].

3.2. The adsorption behavior of samples

In order to explore the adsorption behavior, the equilibration time should be defined firstly. The adsorption capacity of C-BNNP and BNNP with different contact time are investigated and the results are shown in [Fig. 4](#). As shown in [Fig. 4a](#), the adsorption capacity of RhB onto C-BNNP is obviously higher than that onto BNNP and active carbon. And C-BNNP exhibits a best adsorption ability for RhB among the three adsorbents. With the increasing of contact time, the adsorption capacity of RhB onto C-BNNP increases, then the adsorption capacity reaches the maximum value and remains constant after 120 min. The same trend is obtained for BNNP. The adsorption of RhB onto C-BNNP and BNNP can be reached equilibrium in approximately 120 min at room temperature. [Fig. 4b](#) shows the UV-vis absorption spectra of the aqueous solutions of RhB (100 mg/L, 10 mL), in the presence of C-BNNP at different intervals, which indicates C-BNNP can remove RhB from water efficiently within a shot time.

It can be found that doping carbon leads to the enhancement of the adsorption capacity. The reason may be discussed as follows. BNNP is most likely to accept electrons because of the empty orbitals of boron atom [39], and there are lone pair electrons in the oxygen atoms of RhB. Therefore, the electronic properties of

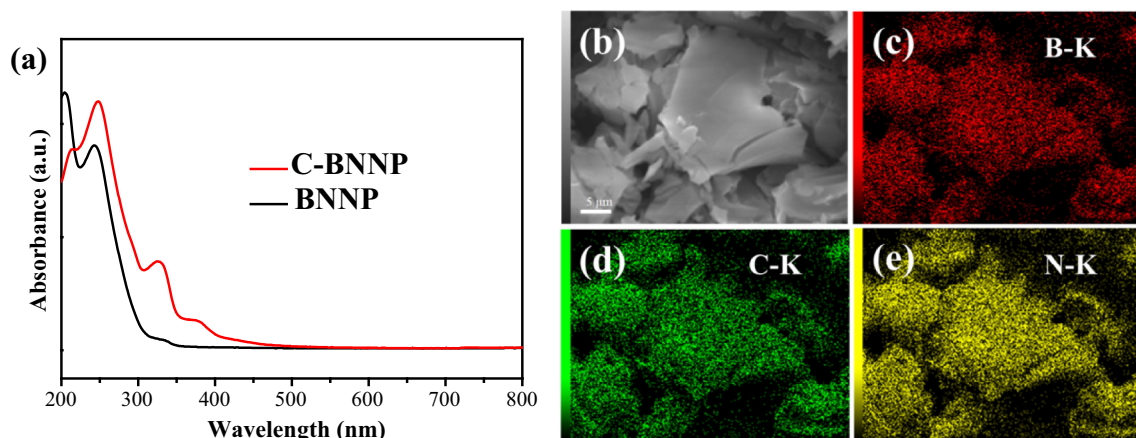


Fig. 2. (a) Ultraviolet–visible diffuse reflectance spectra (UV–vis DRS) of C-BNNP and BNNP, (b) Low-magnified SEM image of C-BNNP, (c–e) Corresponding EDS mapping images of C-BNNP.

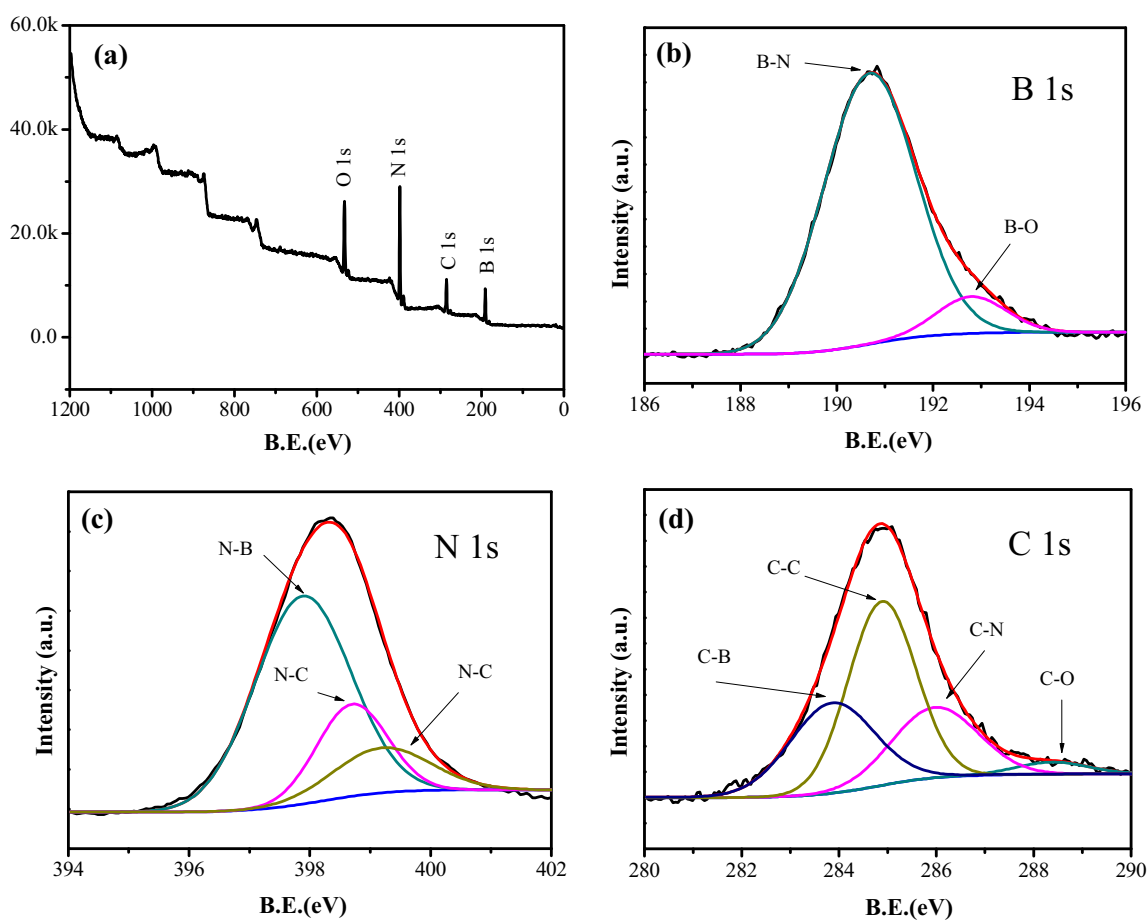


Fig. 3. XPS spectra of C-BNNP.

BNNP are crucial to analyze the interaction between BNNP and RhB. So density functional theory (DFT) is used to investigate the change of electronic properties while carbon atom is doped into BNNP. The structures of C-BNNP and BNNP are constructed for modeling the BN mono-layer. B3LYP/6-311G (2d) is used to obtain the chemical hardness, calculated by the HOMO-LUMO gap. All the calculations are carried out using the Gaussian 09 program. The atom ratio of B, C, N are obtained according to the results given

by XPS data. The optimized structures are shown in [Supplementary Material Fig. S3](#). The HOMO-LUMO gap of C-BNNP and BNNP getting from the optimization are 0.1735 au and 0.2467 au, respectively. Doping carbon atom in the BNNP could decrease the chemical hardness and make it easier to accept electrons. Then the interaction between C-BNNP and RhB would be also stronger and result in the enhanced adsorption capacity. Similar results can also be found in the previous literature [27].

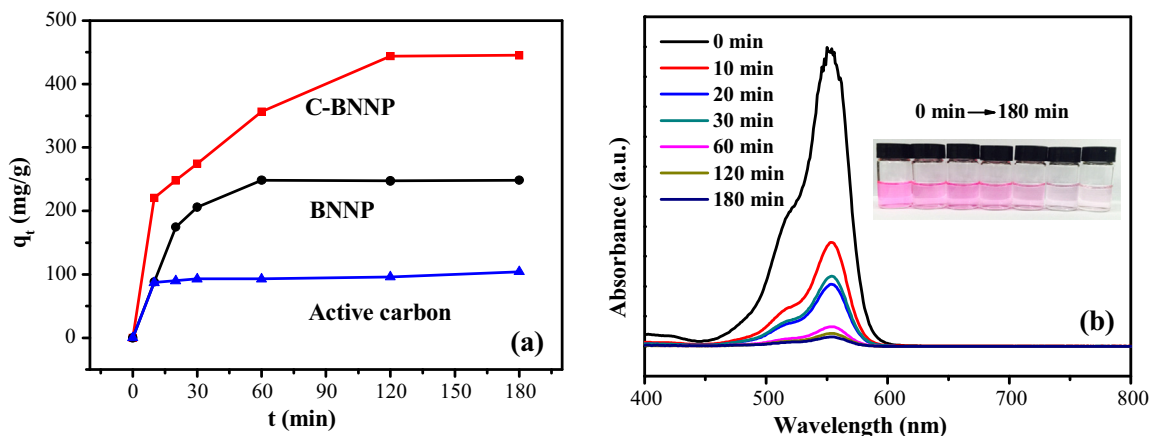


Fig. 4. (a) Effect of adsorption time on the adsorption capacity of RhB onto C-BNNP, BNNP and active carbon. (b) UV-vis absorption spectra of the aqueous solutions of RhB (100 mg/L, 10 ml), in the presence of C-BNNP at different intervals.

3.3. Adsorption kinetics

To explore the adsorption kinetics and understand the mechanism during the adsorption process, the pseudo-first-order and pseudo-second-order kinetics models are used to analyze the data of RhB adsorption onto C-BNNP and BNNP.

The linear form of the pseudo-first-order and pseudo-second-order kinetics model equations are expressed as:

Pseudo-first-order kinetics:

$$\lg(q_e - q_t) = \lg q_e - k_1 t \quad (3)$$

Pseudo-second-order kinetics:

$$\frac{t}{q_t} = \frac{1}{k_2 q_e^2} + \frac{t}{q_e} \quad (4)$$

where q_t and q_e (mg/g) are the adsorption capacity at time t and equilibrium time, respectively, and k_1 (min^{-1}) and k_2 ($\text{g} \cdot \text{mg}^{-1} \cdot \text{min}^{-1}$) are the rate constant of pseudo-first-order model and the pseudo-second order model, respectively. The corresponding kinetic adsorption parameters calculated from the above two kinetic models are listed in Table 1. It can be observed that pseudo-second-order model fits better than pseudo-first-order model according to the correlation coefficient R^2 for the adsorption of RhB onto both C-BNNP and BNNP. Therefore, adsorption behavior can be described properly with the pseudo-second-order model. Moreover the initial adsorption rate (h) and k_2 of BNNP are larger than that of C-BNNP, indicated that the adsorption rate of BNNP is faster than C-BNNP. This probably because larger volume of pore available for the diffusion and transport of RhB [40]. Nevertheless, the C-BNNP shows much higher adsorption capacity than BNNP.

3.4. Adsorption isotherms

The adsorption equilibrium isotherm illuminates the diffusion of adsorbate molecules between the liquid and adsorbent when the adsorption process reached equilibrium state.

The Langmuir isotherm model can be used to describe the assumption of monolayer adsorption systems. The equation can be expressed as:

$$\frac{C_e}{q_e} = \frac{C_e}{q_m} + \frac{1}{q_m K_L} \quad (5)$$

where C_e (mg/L) is the equilibrium concentration of RhB, q_e (mg/L) is the adsorption capacity at the equilibrium point, q_m (mg/g) is the maximum adsorption capacity, K_L is the Langmuir constant.

The Freundlich isotherm model is based on the heterogeneous surfaces and illustrates the multilayer adsorption process. The model is represented in equation:

$$q_e = K_F C_e^{1/n} \quad (6)$$

where C_e and q_e are as defined above, K_F is the Freundlich constant, n is the adsorption intensity.

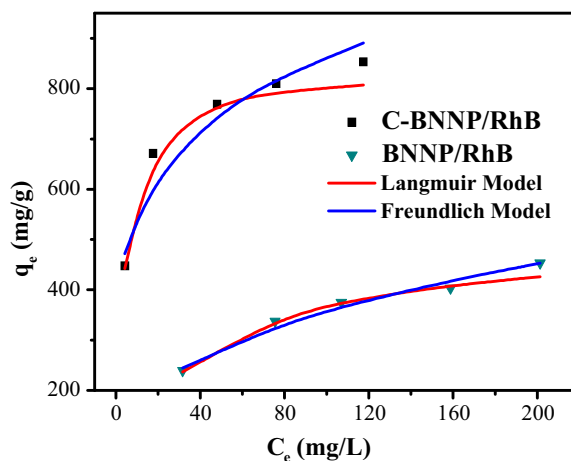


Fig. 5. Two adsorption isotherm models fitted to the experimental data for the adsorption of RhB onto C-BNNP and BNNP, respectively.

Table 1
Kinetics parameters for the adsorption of RhB onto C-BNNP and BNNP.

	Pseudo-first-order			Pseudo-second-order				
	q_m (mg/g)	K_1 (min^{-1})	R^2	q_e (mg/g)	k_2 ($\text{g} \cdot \text{mg}^{-1} \cdot \text{min}^{-1}$)	h ($\text{mg} \cdot \text{g}^{-1} \cdot \text{min}^{-1}$)	$t_{1/2}$ (min)	R^2
C-BNNP	358.63	$6.00 \cdot 10^{-4}$	0.77	500	$0.98 \cdot 10^{-4}$	24.45	20.45	0.99
BNNP	90.07	0.01	0.59	270	$3.57 \cdot 10^{-4}$	26.04	10.32	0.99

Table 2
Langmuir and Freundlich isotherm parameters for the adsorption of RhB onto C-BNNP and BNNP, respectively.

	Langmuir model				Freundlich model			
	q_m (mg/g)	K_L (L/mg)	R^2	APE	n	K_f (L/mg)	R^2	APE
C-BNNP	833	0.26	0.99	$2.21 \cdot 10^{-2}$	5.20	356.02	0.96	$4.26 \cdot 10^{-2}$
BNNP	500	0.03	0.99	$2.01 \cdot 10^{-2}$	3.00	77.13	0.98	$2.32 \cdot 10^{-2}$

Table 3
Langmuir and Freundlich isotherm parameters for the adsorption of RhB on to C-BNNP at different temperature.

T (K)	Langmuir model				Freundlich model			
	q_m (mg/g)	K_L (L/mg)	R^2	APE	n	K_f (L/mg)	R^2	APE
298	833	0.26	0.99	$2.21 \cdot 10^{-2}$	5.20	356.02	0.95	$4.26 \cdot 10^{-2}$
308	769	0.07	0.99	$1.88 \cdot 10^{-2}$	4.07	216.61	0.97	$2.96 \cdot 10^{-2}$
318	714	0.29	0.99	$2.32 \cdot 10^{-2}$	6.36	332.89	0.97	$2.35 \cdot 10^{-2}$

The average percentage error (APE) is written as:

$$APE = \sum_{i=1}^N |(q_{e,exp} - q_{e,cal})/q_{e,exp}|/N \quad (7)$$

Where $q_{e,exp}$ and $q_{e,cal}$ are the adsorption capacity of experimental value and calculated value by the isotherm models, respectively. N is the number of experiment data point. The plot of q_e versus C_e is shown in Fig. 5. According to the coefficients R^2 and APE of the adsorption isotherm parameters presented in Table 2, the adsorption equilibrium data fit better with the Langmuir isotherm, suggesting that the adsorption behaviors of both C-BNNP and BNNP for the RhB are probably the monolayer molecular adsorption. The maximum adsorption capacity of C-BNNP for RhB is 833 mg/g, which is larger than that of BNNP (500 mg/g), and is much higher than most of those reported adsorbents listed in Supplementary Material Table S2.

The adsorption isotherms for RhB onto C-BNNP at different temperature (298, 308, 318 K) are also investigated. The results are shown in Table 3. q_m of RhB presents a decreasing trend with the

increasing of temperature. It suggests that RhB adsorption onto the C-BNNP is favored at lower temperature in the chosen temperature range. The reason may be supposed that the adsorption of RhB onto C-BNNP is an exothermic process. High temperature does not promote the adsorption capacity in this system.

3.5. Adsorption thermodynamics

The Vant Hoff analysis [41] is used to illustrate the spontaneity of the RhB adsorption onto the C-BNNP and calculate various thermodynamic parameters by the following equations [42].

$$\Delta G = -RT \ln K_c \quad (8)$$

$$\ln K_c = \frac{\Delta S}{R} - \frac{\Delta H}{RT} \quad (9)$$

$$\Delta S = \frac{\Delta H - \Delta G}{T} \quad (10)$$

where ΔG is the change in Gibbs free energy ($\text{J} \cdot \text{mol}^{-1}$), ΔH is the change in enthalpy ($\text{J} \cdot \text{mol}^{-1}$), ΔS is the change in entropy ($\text{J} \cdot \text{mol}^{-1} \cdot \text{K}^{-1}$), R is universal gas constant ($8.314 \text{ J} \cdot \text{K}^{-1} \cdot \text{mol}^{-1}$), T is the temperature (K), and $\ln K_c = q_e/C_e$.

The thermodynamic parameters are reported in Table 4. ΔG for different temperatures are negative, indicating that the adsorption of RhB onto C-BNNP is a spontaneous process [43]. The negative values of ΔH indicate the exothermic process. In addition, the results of ΔG values are between -20 kJ/mol and 0 kJ/mol , revealing that the process is dominated by physical adsorption [44]. The negative values of ΔS suggest that the randomness at the solid/solution interface decreases gradually accompanied by the creation of the affinity of C-BNNP towards RhB [45]. Thus, more ordered arrangement of RhB molecules shape on C-BNNP surface.

3.6. Regeneration study

Regeneration capacity of an adsorbent decides the cost of operation and plays a significant role in the practical application. Fig. 6 illustrates the regeneration behavior of C-BNNP upon RhB for five cycles. It can be seen that the C-BNNP could remain almost the same adsorption capacity and still remains 98% after 5 cycles, indicating that the prepared adsorbents is promising to be a potential candidate for industrial applications.

Table 4
Thermodynamic parameters for the RhB adsorption onto C-BNNP.

T (K)	ΔG (kJ/mol)	ΔH (kJ/mol)	ΔS (J/(mol·K))	R^2
298	-4.86	-16.44	-38.92	0.99
308	-4.38			
318	-4.09			

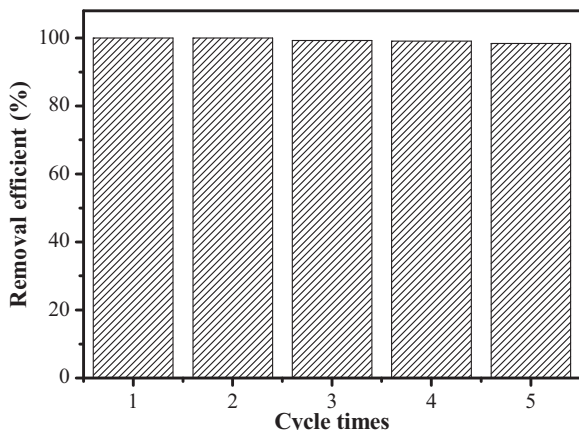


Fig. 6. Recyclability of the C-BNNP for adsorption RhB.

4. Conclusions

In summary, C-BNNP has been synthesized successfully and proves superior adsorption capacity for RhB. Results show that C-BNNP exhibits greater adsorption capacity (833 mg/g) for RhB than that of BNNP (500 mg/g). The data obey the pseudo-second-order model. And the adsorption isotherms exhibit a better fit with the Langmuir model than the Freundlich model, suggesting that sorption of dyes on C-BNNP proceeds through monolayer coverage. The thermodynamic suggests that the adsorption process is spontaneous ($\Delta G < 0$) and exothermic ($\Delta H < 0$). Doping carbon in the BNNP decreases the chemical hardness and enhances the interaction between C-BNNP and RhB. It's expected tuning electronic properties by doping atom can be an efficient strategy to enhance adsorptive performance.

Acknowledgments

The authors are grateful for financial supported by the National Nature Science Foundation of China (Nos. 21506083, 21576122, 21646001). Postdoctoral Innovation Fund of China and Jiangsu Province (2017M611726, 1601254C). Doctoral Innovation Fund of Jiangsu Province (KYLX16_0915). Key Laboratory of Tropical Medicinal Plant Chemistry of Ministry of Education, Hainan Normal University (20150376).

Appendix A. Supplementary material

Supplementary data associated with this article can be found, in the online version, at <http://dx.doi.org/10.1016/j.jcis.2017.08.012>.

References

- [1] S.K. Gupta, M.K. Nayunigari, R. Misra, F.A. Ansari, D.D. Dionysiou, A. Maity, F. Bux, Synthesis and performance evaluation of a new polymeric composite for the treatment of textile wastewater, *Ind. Eng. Chem. Res.* 55 (2016) 13–20.
- [2] S. Sansuk, S. Srijaranai, S. Srijaranai, A new approach for removing anionic organic dyes from wastewater based on electrostatically driven assembly, *Environ. Sci. Technol.* 50 (2016) 6477–6484.
- [3] F. Martin, J.M. Oberson, M. Meschiari, C. Munari, Determination of 18 water-soluble artificial dyes by LC-MS in selected matrices, *Food Chem.* 197 (2016) 1249–1255.
- [4] M. Norman, P. Bartczak, J. Zdarta, H. Ehrlich, T. Jesionowski, Anthocyanin dye conjugated with *Hippospongia communis* marine demersal sponge skeleton and its antiradical activity, *Dyes Pigm.* 134 (2016) 541–552.
- [5] Y. Li, W.Q. Cui, L. Liu, R.L. Zong, W.Q. Yao, Y.H. Liang, Y.F. Zhu, Removal of Cr(VI) by 3D TiO₂-graphene hydrogel via adsorption enriched with photocatalytic reduction, *Appl. Catal. B: Environ.* 199 (2016) 412–423.
- [6] S.J. You, B. Liu, Y.F. Gao, Y. Wang, C.Y. Tang, Y.B. Huang, N.Q. Ren, Monolithic porous magneli-phase Ti₄O₇ for electro-oxidation treatment of industrial wastewater, *Electrochim. Acta* 214 (2016) 326–335.
- [7] W. Cheng, F. Rechberger, M. Niederberger, Three-dimensional assembly of yttrium oxide nanosheets into luminescent aerogel monoliths with outstanding adsorption properties, *ACS Nano* 10 (2016) 2467–2475.
- [8] A. Alsaiee, B.J. Smith, L.L. Xiao, Y.H. Ling, D.E. Helbling, W.R. Dichtel, Rapid removal of organic micropollutants from water by a porous beta-cyclodextrin polymer, *Nature* 529 (2016) 190–194.
- [9] P. Tan, J.X. Qin, X.Q. Liu, X.Q. Yin, L.B. Sun, Fabrication of magnetically responsive core-shell adsorbents for thiophene capture: AgNO₃-functionalized Fe₃O₄@mesoporous SiO₂ microspheres, *J. Mater. Chem. A* 2 (2014) 4698–4705.
- [10] J.X. Qin, P. Tan, Y. Jiang, X.Q. Liu, Q.X. He, L.B. Sun, Functionalization of metal-organic frameworks with cuprous sites using vapor-induced selective reduction: efficient adsorbents for deep desulfurization, *Green Chem.* 18 (2016) 3210–3215.
- [11] S. Qu, F. Huang, S.N. Yu, G. Chen, J.L. Kong, Magnetic removal of dyes from aqueous solution using multi-walled carbon nanotubes filled with Fe₂O₃ particles, *J. Hazard. Mater.* 160 (2008) 643–647.
- [12] A. Bayat, S.F. Aghamiri, A. Moheb, G.R. Vakili-Nezhaad, Oil spill cleanup from sea water by sorbent materials, *Chem. Eng. Technol.* 28 (2005) 1525–1528.
- [13] Y. Yu, J.G. Shapter, R. Popelka-Filcoff, J.W. Bennett, A.V. Ellis, Copper removal using bio-inspired polydopamine coated natural zeolites, *J. Hazard. Mater.* 273 (2014) 174–182.
- [14] A. Rahman, N. Kishimoto, T. Urabe, Adsorption characteristics of clay adsorbents-sepiolite, kaolin and synthetic talc-for removal of Reactive Yellow 138:1, *Water Environ. J.* 29 (2015) 375–382.
- [15] W.S. Zhu, X. Gao, Q. Li, H.P. Li, Y.H. Chao, M.J. Li, S.M. Mahurin, H.M. Li, H.Y. Zhu, S. Dai, Controlled gas exfoliation of boron nitride into few-layered nanosheets, *Angew. Chem. Int. Ed.* 55 (2016) 10766–10770.
- [16] C.J. Huang, C. Chen, M.W. Zhang, L.H. Lin, X.X. Ye, S. Lin, M. Antonietti, X.C. Wang, Carbon-doped BN nanosheets for metal-free photoredox catalysis, *Nat. Commun.* 6 (2015) 7698–7704.
- [17] G. Gautam, C.S. Tiwary, S. Lose, G. Brunetto, S. Ozden, S. Vinod, P. Raghavan, S. Biradar, D.S. Galvao, P.M. Ajayan, Synthesis of low-density, carbon-doped, porous hexagonal boron nitride solids, *ACS Nano* 9 (2015) 12088–12095.
- [18] J. Xiong, L. Yang, Y.H. Chao, J.Y. Pang, M. Zhang, W.S. Zhu, H.M. Li, Boron nitride mesoporous nanowires with doped oxygen atoms for the remarkable adsorption desulfurization performance from fuels, *ACS Sustain. Chem. Eng.* 4 (2016) 4457–4464.
- [19] J. Xiong, W.S. Zhu, H.P. Li, W.J. Ding, Y.H. Chao, P.W. Wu, S.H. Xun, M. Zhang, H. M. Li, Few-layered graphene-like boron nitride induced a remarkable adsorption capacity for dibenzothiophene in fuels, *Green Chem.* 17 (2015) 1647–1656.
- [20] Y.H. Chao, W.S. Zhu, J.X. Chen, P.W. Wu, X.Y. Wu, H.M. Li, C.R. Han, S. Yan, Development of novel graphene-like layered hexagonal boron nitride for adsorptive removal of antibiotic gatifloxacin from aqueous solution, *Green Chem. Lett. Rev.* 7 (2014) 330–336.
- [21] W.W. Lei, D. Portehault, D. Liu, S. Qin, Y. Chen, Porous boron nitride nanosheets for effective water cleaning, *Nat. Commun.* 4 (2013) 1777–1783.
- [22] W.W. Lei, D. Liu, Y. Chen, Highly crumpled boron nitride nanosheets as adsorbents: scalable solvent-less production, *Adv. Mater. Interfaces* 2 (2015) 1400529–1400534.
- [23] J. Lin, L.L. Xu, Y. Huang, J. Li, W.J. Wang, C.C. Feng, Z.Y. Liu, X.W. Xu, J. Zou, C.C. Tang, Ultrafine porous boron nitride nanofibers synthesized via a freeze-drying and pyrolysis process and their adsorption properties, *RSC Adv.* 6 (2016) 1253–1259.
- [24] J. Li, X. Xiao, X.W. Xu, J. Lin, Y. Huang, Y.M. Xue, P. Jin, J. Zou, C.C. Tang, Activated boron nitride as an effective adsorbent for metal ions and organic pollutants, *Sci. Rep.* 3 (2013) 3208–3214.
- [25] J. Li, H.C. Jia, J. Lin, H. Luo, Z.Y. Liu, X.W. Xu, Y. Huang, P. Jin, J. Zhang, S. Abbas, C. C. Tang, Free-standing membranes made of activated boron nitride for efficient water cleaning, *RSC Adv.* 5 (2015) 71537–71543.
- [26] F. Liu, J. Yu, X.X. Ji, M.Q. Qian, Nanosheet-structured boron nitride spheres with a versatile adsorption capacity for water cleaning, *ACS Appl. Mater. Interfaces* 7 (2015) 1824–1832.
- [27] H.P. Li, W.S. Zhu, S.W. Zhu, J.X. Xia, Y.H. Chang, W. Jiang, M. Zhang, Y.W. Zhou, H.M. Li, The selectivity for sulfur removal from oils: an insight from conceptual density functional theory, *AIChE J.* 62 (2016) 2087–2100.
- [28] A. Pakdel, Y. Bando, D. Golberg, Nano boron nitride flatland, *Chem. Soc. Rev.* 43 (2014) 934–959.
- [29] Q.H. Weng, X.B. Wang, X. Wang, Y.S. Bando, D. Golberg, Functionalized hexagonal boron nitride nanomaterials: emerging properties and applications, *Chem. Soc. Rev.* 45 (2016) 3989–4012.
- [30] P.W. Wu, W.S. Zhu, Y.H. Chao, J.S. Zhang, P.F. Zhang, H.Y. Zhu, C.F. Li, Z.G. Chen, H.M. Li, S. Dai, A template-free solvent-mediated synthesis of high surface area boron nitride nanosheets for aerobic oxidative desulfurization, *Chem. Commun.* 52 (2016) 144–147.
- [31] F. Liu, X.S. Mo, H.B. Gan, T.Y. Guo, X.B. Wang, B. Chen, J. Chen, S.Z. Deng, N.S. Xu, T. Sekiguchi, D. Golberg, Y. Bando, Cheap, gram-scale fabrication of BN nanosheets via substitution reaction of graphite powders and their use for mechanical reinforcement of polymers, *Sci. Rep.* 4 (2014) 4211–4218.
- [32] F. Xiao, Z.X. Chen, G. Casillas, C. Richardson, H.J. Li, Z.G. Huang, Controllable synthesis of few-layered and hierarchically porous boron nitride nanosheets, *Chem. Commun.* 52 (2016) 3911–3914.
- [33] C.J. Huang, C. Chen, X.X. Ye, W.Q. Ye, J.L. Hu, C. Xu, X.Q. Qiu, Stable colloidal boron nitride nanosheet dispersion and its potential application in catalysis, *J. Mater. Chem. A* 1 (2013) 12192–12197.
- [34] A. Pakdel, X.B. Wang, C.Y. Zhi, Y. Bando, K. Watanabe, T. Sekiguchi, T. Nakayama, D. Golberg, Facile synthesis of vertically aligned hexagonal boron nitride nanosheets hybridized with graphitic domains, *J. Mater. Chem.* 22 (2012) 4818–4824.
- [35] X.B. Chen, C. Burda, The electronic origin of the visible-light absorption properties of C-, N- and S-doped TiO₂ nanomaterials, *J. Am. Chem. Soc.* 130 (2008) 5018–5019.
- [36] Y.J. Zhang, T. Mori, J.H. Ye, M. Antonietti, Phosphorus-doped carbon nitride solid: Enhanced electrical conductivity and photocurrent generation, *J. Am. Chem. Soc.* 132 (2010) 6294–6295.
- [37] E. Iyyamperumal, S. Wang, L. Dai, Vertically aligned BCN nanotubes with high capacitance, *ACS Nano* 6 (2012) 5259–5265.
- [38] J.S. Zhou, N. Li, F.M. Gao, Y.F. Zhao, L. Hou, Z.M. Xu, Vertically-aligned BCN nanotube arrays with superior performance in electrochemical capacitors, *Sci. Rep.* 4 (2014) 6083–6088.
- [39] D. Liu, W.W. Lei, S. Qin, K.D. Klika, Y. Chen, Superior adsorption of pharmaceutical molecules by highly porous BN nanosheets, *Phys. Chem. Chem. Phys.* 18 (2016) 84–88.
- [40] Y. Shen, X.Y. Zhu, B.L. Chen, Size effects of graphene oxide nanosheets on the construction of three-dimensional graphene-based macrostructures as adsorbents, *J. Mater. Chem. A* 4 (2016) 12106–12118.
- [41] Y.H. Chao, W.S. Zhu, X.Y. Wu, F.F. Hou, S.H. Xun, P.W. Wu, H.Y. Ji, H. Xu, H.M. Li, Application of graphene-like layered molybdenum disulfide and its excellent adsorption behavior for doxycycline antibiotic, *Chem. Eng. J.* 243 (2014) 60–67.

- [42] A.S. Patra, S. Ghorai, S. Ghosh, B. Mandal, S. Pal, Selective removal of toxic anionic dyes using a novel nanocomposite derived from cationically modified guar gum and silica nanoparticles, *J. Hazard. Mater.* 301 (2016) 127–136.
- [43] X.X. Liu, J. Luo, Y.T. Zhu, Y. Yang, S.J. Yang, Removal of methylene blue from aqueous solutions by an adsorbent based on metal-organic framework and polyoxometalate, *J. Alloys Compd.* 648 (2015) 986–993.
- [44] J.X. Shu, Z.H. Wang, Y.J. Huang, N. Huang, C.G. Ren, W. Zhang, Adsorption removal of Congo red from aqueous solution by polyhedral Cu_2O nanoparticles: Kinetics, isotherms, thermodynamics and mechanism analysis, *J. Alloys Compd.* 633 (2015) 338–346.
- [45] A.A. Farghali, M. Bahgat, W.M.A. El Roubay, M.H. Khedr, Preparation, decoration and characterization of graphene sheets for methyl green adsorption, *J. Alloys Compd.* 555 (2013) 193–200.